Receptor-like cytoplasmic kinase MARIS functions downstream of *Cr*RLK1L-dependent signaling during tip growth

Aurélien Boisson-Dernier[a,b,c,1], Christina Maria Franck[a,b,c], Dmytro S. Lituiev (Дмитро Сергійович Літуєв)[b,c], and Ueli Grossniklaus[b,c]

[a]Biocenter, Botanical Institute, University of Cologne, 50674 Cologne, Germany; [b]Institute of Plant Biology, University of Zurich, 8008 Zurich, Switzerland; and [c]Zurich-Basel Plant Science Center, University of Zurich, 8008 Zurich, Switzerland

Edited by June B. Nasrallah, Cornell University, Ithaca, NY, and approved August 26, 2015 (received for review June 24, 2015)

Growing plant cells need to rigorously coordinate external signals with internal processes. For instance, the maintenance of cell wall (CW) integrity requires the coordination of CW sensing with CW remodeling and biosynthesis to avoid growth arrest or integrity loss. Despite the involvement of receptor-like kinases (RLKs) of the *Catharanthus roseus* RLK1-like (*Cr*RLK1L) subfamily and the reactive oxygen species-producing NADPH oxidases, it remains largely unknown how this coordination is achieved. ANXUR1 (ANX1) and ANX2, two redundant members of the *Cr*RLK1L subfamily, are required for tip growth of the pollen tube (PT), and their closest homolog, FERONIA, controls root-hair tip growth. Previously, we showed that ANX1 overexpression mildly inhibits PT growth by oversecretion of CW material, whereas pollen tubes of *anx1 anx2* double mutants burst spontaneously after germination. Here, we report the identification of suppressor mutants with improved fertility caused by the rescue of *anx1 anx2* pollen tube bursting. Mapping of one these mutants revealed an R240C nonsynonymous substitution in the activation loop of a receptor-like cytoplasmic kinase (RLCK), which we named MARIS (MRI). We show that MRI is a plasma membrane-localized member of the RLCK-VIII subfamily and is preferentially expressed in both PTs and root hairs. Interestingly, *mri*-knockout mutants display spontaneous PT and root-hair bursting. Moreover, expression of the MRI^{R240C} mutant, but not its wild-type form, partially rescues the bursting phenotypes of *anx1 anx2* PTs and *fer* root hairs but strongly inhibits wild-type tip growth. Thus, our findings identify a novel positive component of the *Cr*RLK1L-dependent signaling cascade that coordinates CW integrity and tip growth.

receptor-like kinase signaling | cell wall integrity | pollen tube | root hair | *Arabidopsis*

Growing plant cells are in constant communication with their environment, monitoring external signals that lead to internal reactions. Because cellular growth depends on a tight coordination of external and internal processes, signaling between the extracellular matrix, i.e., the primary cell wall (CW), and the internal growth machinery plays a central role in its regulation. The turgor pressure-resisting CW that shields plant cells from a changing environment exhibits remarkable but seemingly contradictory properties: rigidity and extensibility. Growing cells must find a balance between loosening their CWs sufficiently to allow expansion but not so much that they lose CW integrity. Because any environmental perturbation affecting the properties of the CW can upset this fragile balance, plant cells have developed complex sensing mechanisms to coordinate the state of the CW with the internal growth machinery (1, 2). These CW sensing mechanisms must be particularly robust in fast-growing cells, such as the tip-growing root hairs and pollen tubes (PTs), the male gametophytes of flowering plants. PTs elongate rapidly and grow over long distances within female tissues to deliver the sperm cells to the female gametophytes, which are deeply embedded in the ovules. Considering the vast excess of pollen grains that germinate on a receptive stigma, there is strong competition, and PTs must grow as fast as possible to reach unfertilized ovules; otherwise they will not contribute to the next generation. However, PTs must ensure that, while elongating extremely rapidly, they do not lose their integrity. In PTs of the model plant *Arabidopsis thaliana*, the plasma membrane-localized ANXUR (ANX1 and ANX2) receptor-like kinases (RLKs) play a major role in controlling CW integrity and growth. On one hand, loss of function of the redundant RLKs ANX1 and ANX2 leads to precocious PT rupture shortly after germination, resulting in male sterility (3, 4). This phenotype also is seen when the ANX-RLKs are degraded by the endoplasmic reticulum-associated degradation pathway in the *turan* mutant affecting N-glycosylation (5). On the other hand, overexpression of ANX-RLKs inhibits pollen germination and PT elongation, most likely because of the oversecretion of CW material (6). The ANX-RLKs and their closest homolog FERONIA (FER) belong to the *Catharanthus roseus* RLK1-like (*Cr*RLK1L) subfamily that has been investigated extensively as putative CW sensors involved in coordinating cell growth, cell–cell communication, defense against pathogens, and hormone signaling as well as CW remodeling and integrity (reviewed in refs. 7–9). FER, the most thoroughly studied member of this subfamily, controls many developmental processes, such as intercellular communication during fertilization (10–12), cell elongation (13), calcium and hormone signaling (10, 14, 15), mechanosensing (16), plant

Significance

Plant cells constantly survey their environment to fine-tune their internal processes. Plant receptor-like kinases (RLKs) of the *Catharanthus roseus* RLK1-like (*Cr*RLK1L) subfamily have been implicated in many signaling processes, including the coordination of the intracellular growth machinery with the performance of the extracellular matrix, i.e. the cell wall (CW). To avoid loss of integrity and growth and to adapt their CWs to developmental and environmental perturbations, growing plant cells have developed complex sensing mechanisms. The *Cr*RLK1Ls ANXUR1 and ANXUR2 and their closest homolog FERONIA control CW integrity in the tip-growing pollen tubes and root hairs, respectively. Here, we identify and characterize the receptor-like cytoplasmic kinase MARIS as a novel downstream component of the *Cr*RLK1L-dependent signaling cascade that controls CW integrity in tip-growing cells.

Author contributions: A.B.-D. and U.G. designed research; A.B.-D., C.M.F., and D.S.L. performed research; U.G. contributed new reagents/analytic tools; A.B.-D., C.M.F., and D.S.L. analyzed data; and A.B.-D. wrote the paper with help from U.G.

The authors declare no conflict of interest.

This article is a PNAS Direct Submission.

[1]To whom correspondence should be addressed. Email: aboisson@uni-koeln.de.

This article contains supporting information online at www.pnas.org/lookup/suppl/doi:10.1073/pnas.1512375112/-/DCSupplemental.

defense (17, 18), and growth control of root hairs (19). Despite the many reports describing the role of *Cr*RLK1Ls in various signaling processes, the mechanistic basis of their function and their relationship with other pathways remain poorly understood. FER was recently found to mediate the inhibition of primary root growth by forming a receptor–ligand pair with the rapid alkalinization factor 1 (RALF1) peptide (20). Moreover, it was shown that the intracellular kinase domains of three *Cr*RLK1Ls members are interchangeable and that the various *Cr*RLK1Ls share downstream signaling components (21). This finding has been confirmed for at least one signaling component so far, namely the reactive oxygen species (ROS)-producing NADPH oxidases, also called "respiratory burst oxidase homologs" (Rboh). It was reported that RbohD/RbohF for THESEUS1 (THE1), RbohC for FER, and RbohH/RbohJ for ANX1/2 act downstream of the *Cr*RLK1Ls in primary roots, root hairs, and PTs, respectively (6, 19, 22).

Here, we report, based on an *anx1 anx2* male sterility suppressor screen, the identification of the receptor-like cytoplasmic kinase (RLCK) MARIS (MRI), a novel component of the *Cr*RLK1L-mediated signaling pathway in tip-growing cells. *MRI* is expressed preferentially in PTs and root hairs, and its disruption triggers spontaneous bursting of PTs and root hairs. The suppressor mutant carries a R240C amino acid substitution in the activation loop of MRI. Expression of MRI^{R240C} partially rescues the bursting phenotypes of *anx1 anx2* and *rbohH rbohJ* PTs as well as *fer* root hairs while strongly inhibiting WT tip growth, indicating that this mutant form of MRI overactivates the *Cr*RLK1L-dependent pathway downstream of the NADPH oxidases.

Results

An anx1 anx2 Sterility-Suppressor Screen Identifies Putative Components of the ANX1/2 Pathway. To identify putative downstream components of the *ANX1/2* pathway, a forward genetic screen to identify suppressor mutations of the *anx1 anx2* PT-bursting phenotype was carried out (Fig. 1*A*). We anticipated that rescue of *anx1 anx2* PT bursting in vivo by a second site mutation would lead to improved plant fertility characterized by elongated siliques, an easily scorable phenotype. Approximately 7,000 ethyl-methyl sulfonate (EMS)-treated *anx1-2 anx2-2* M1 plants were screened for silique elongation, resulting in the identification of ∼30 suppressor mutants, all of which were confirmed to be true double homozygous *anx1-2 anx2-2* plants. In all these plants, aniline-blue staining showed rescue of *anx1-2 anx2-2* PT growth in vivo as well as normal targeting of unfertilized ovules (Fig. 1*B*). Backcrosses of the M1 mutants as pollen donor on the stigmas of the original *anx1-2 anx2-2* plants systematically led to elongated siliques, showing that the rescue of PT growth was caused by mutation(s) in the haploid male gametophyte, thus defining the *impotence rescued* (*ipr*) class of mutants. Here, we report the identification of one of these *ipr* mutants, which we named "*maris*" (*mri-3D*; see below) after the Etruscan god of fertility and agriculture (23). The *mri-3D* suppressor mutation restores in vivo growth of *anx1 anx2* PTs, resulting in filled siliques (43 ± 5.4 seeds for *mri-3D* compared with less than one seed for *anx1 anx2* siliques) (Fig. 1*B*). To identify the EMS-generated causative lesion in *mri-3D,* likely a single nucleotide polymorphism (SNP), an SNP-ratio mapping (SRM) approach (24), was carried out with modifications (*SI Material and Methods*). Briefly, the SNPs called with Freebayes were fed to a hidden Markov chain-based algorithm that estimates the probability that the SNP is the causative SNP, based on the read data and linkage between the SNPs within each chromosome. For *mri-3D/MRI*, the top candidate exonic SNP had a ratio of alternate to reference reads of 0.476, very close to the theoretically expected ratio of 0.500 (Datasets S1 and S2) (24). The affected gene *AT2G41970* encodes an uncharacterized RLCK, henceforth referred to as "MARIS" (MRI) (see below). MRI belongs to the family of RLCK-VIII homologs of the tomato Pto-interacting protein 1 (Pti1) and is highly expressed in pollen as well as in roots and root hairs according to publicly available microarray data and previous transcriptomic studies (Fig. S1*A* and Table S1).

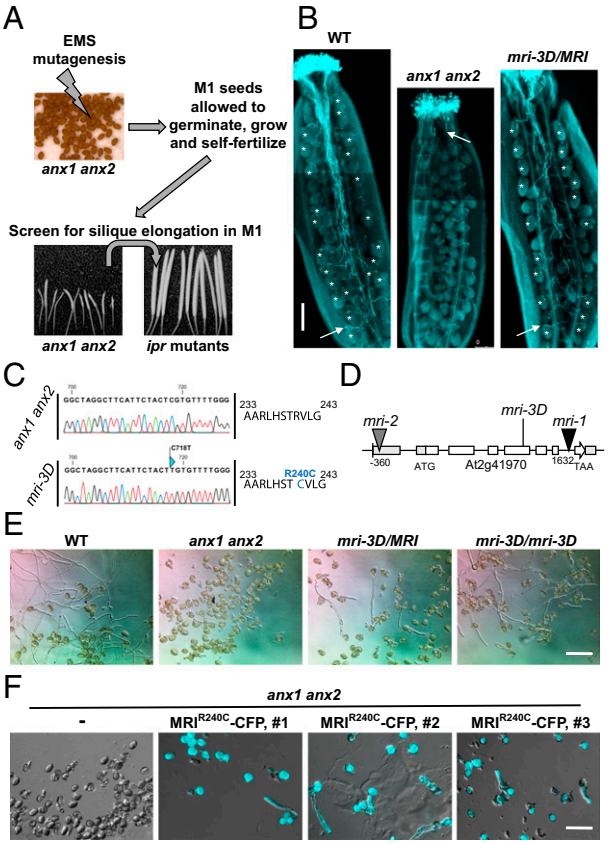

Fig. 1. Identification of the *ipr* mutants, suppressors of *anx1 anx2* male sterility, and characterization of *maris-3D* (*mri-3D*). (*A*) Scheme for the *anx1 anx2* male sterility-suppressor screen. Reproduced from ref. 6. (*B*) Aniline blue staining reveals that *mri-3D/MRI* PTs are able to elongate in vivo and fertilize female gametophytes, unlike *anx1 anx2* PTs, which burst and stop growth early in the style. White arrows indicate the tip of the longest PT. Asterisks indicate female gametophytes normally targeted by PTs. (Scale bar: 200 μm.) (*C*) The *mri-3D* mutant carries a C718T SNP in *AT2G41970* that corresponds to an R240C mutation at the protein level. Shown are spectra from the Sanger sequencing reactions of the *AT2G41970* cDNA amplified from *anx1 anx2* (*Upper*) or *mri-3D anx1 anx2* (*Lower*) flowers. (*D*) *AT2G41970* locus with introns, exons, and positions of the mutant alleles. (*E*) In vitro PT growth assays of WT, *anx1 anx2*, heterozygous *mri-3D/MRI anx1 anx2*, and homozygous *mri-3D/mri-3D anx1 anx2*. Note how the *mri-3D* mutation partially rescues the *anx1 anx2* pollen-bursting phenotype and allows PT growth. See Fig. S2*C* for corresponding quantification. (Scale bar: 100 μm.) (*F*) In vitro PT growth assays of untransformed *anx1 anx2* and three independent *anx1 anx2* transgenic lines expressing MRI^{R240C}-CFP. DIC and CFP channels were overlaid for the transgenic lines. (Scale bar: 80 μm.)

The putative causative SNP in *mri-3D* is a C-to-T transition at position 718 of the coding sequence of *MRI* that leads to a non-synonymous substitution of a perfectly conserved arginine into a cysteine (R240C) in the activation loop of the kinase (Fig. 1*C* and Fig. S1*B*). All mutant plants used for the SRM approach were heterozygous for this SNP (Fig. S2*A*). *mri-3D/MRI* also displayed partial rescue of the *anx1 anx2* PT-bursting phenotype in vitro (Fig. 1*E* and Fig. S2*C*). All the 20 progenies of selfed *mri-3D/MRI* were either heterozygous (n = 12), or homozygous (n = 8) for the causative SNP in *MRI*, suggesting that this mutation confers a reproductive advantage relative to the WT allele in the *anx1 anx2* background (Fig. S2*B*). As expected, in *mri-3D/mri-3D* plants, roughly twice as many PTs were rescued from bursting in *anx1 anx2* plants as in *mri-3D/MRI* plants (Fig. 1*E* and Fig. S2*C*).

To confirm that the mutant form MRI^{R240C} was indeed responsible for the suppression of PT bursting in *anx1 anx2* plants, *anx1/anx1 anx2/ANX2* plants were transformed with MRI^{R240C}-CFP and MRI-CFP fusion constructs under the control of the pollen-specific promoter Lat52 (25) and were compared with previous complementation experiments with ANX1-YFP and ANX2-YFP (6). In the progeny of selfed *anx1/anx1 anx2/ANX2* plants with high MRI-CFP expression levels, no homozygous *anx1 anx2* individuals could be recovered ($n = 85$) (Table S2). In contrast, homozygous *anx1 anx2* individuals could be identified in the self-progeny of *anx1/anx1 anx2/ANX2* plants with high MRI^{R240C}-CFP expression levels ($n = 13$ of 88), similar to the ANX1-YFP and ANX2-YFP fusion proteins ($n = 13$ of 87) (Table S2). Moreover, seed set for three independent MRI^{R240C}-CFP transgenic lines homozygous for *anx1 anx2* was 14.6 ± 4.4, 14.2 ± 2.8, and 14.6 ± 3.2 on average, as opposed to less than one seed from untransformed *anx1 anx2* plants. These results indicate that MRI^{R240C}-CFP, but not MRI-CFP, can partially rescue *anx1 anx2* male sterility in vivo. Furthermore, unlike untransformed *anx1 anx2* plants, pollen of homozygous *anx1 anx2* plants expressing MRI^{R240C}-CFP was able to produce some PTs in vitro, albeit at a lower rate than by the original *mri-3D/MRI* mutant (Fig. 1*F*, three independent lines). These results demonstrate that the MRI^{R240C} mutant protein is indeed responsible for the partial rescue of the *anx1 anx2* PT-bursting phenotype observed in the original *mri-3D* mutant and that MRI^{R240C} exerts a dominant effect over the WT form.

MRI Is a Positive Component of the ANX1/2 Pathway. To understand the role of MRI further, we looked for insertion lines that potentially could disrupt *MRI* function. Two lines were recovered, CSHL_GT21229 (gene trap line, *Ds* transposon, L*er*), renamed "*mri-1*," and GABI_820D05 (T-DNA insertion, Col-0), renamed "*mri-2*" (Fig. 1*D*). Although homozygous *mri-2* individuals could be retrieved from selfed *mri-2/MRI* plants, albeit less often than expected, no homozygous *mri-1* individuals were identified ($n = 353$; Table S3). Moreover, both distortion of the segregation ratio and analysis of transmission efficiency (TE) showed that both *mri-1* and *mri-2* were normally transmitted through the female gametophyte but showed no or reduced transmission, respectively, through the male gametophyte (Table S4). To understand how the *mri-1* and *mri-2* alleles affect pollen development, in vitro pollen germination assays were carried out. Because *mri-1/MRI* was originally in the L*er* accession that is recalcitrant to in vitro pollen germination assays, *mri-1/MRI* was introgressed into the Col-0 background carrying the *quartet* (*qrt*) mutation (26) (*SI Materials and Methods*). Unlike WT segregants, germinated PTs from *mri-1/MRI* quartets either burst ($n = 194$) or grew normally ($n = 160$) in a 1:1 ratio, as expected for the segregating *mri-1* allele (two-tailed Fisher's exact test, $P = 0.2286$) (Fig. 2*A*). Moreover, 64.3% of PTs from *mri-2/mri-2* plants (vs. 14.6% of PTs from WT plants) lost integrity and burst in germination assays, similar to the percentages of bursting PTs from homozygous *rbohH rbohJ* (87.4%) and *anx1 anx2* (100%) plants (Fig. 2 *B* and *C*). Next, we transformed *mri-1/MRI* plants with *pLat52-MRI-YFP* and measured PT bursting in four independent *mri-1/MRI* transgenic T1 lines hemizygous for MRI-YFP. All the lines displayed significantly less PT bursting (30–39%) than untransformed *mri-1/MRI* plants (56%) ($P < 0.001$ for all lines, Student's *t* test) (Fig. 2 *D* and *E*). Moreover, out of 90 plants 29 homozygous *mri-1/mri-1* individuals were identified in the subsequent generation, showing that MRI-YFP is functional.

Although MRI does not possess a transmembrane domain, MRI-YFP localized to the plasma membrane of growing PTs, possibly through palmitoylation (Fig. 2*F*). However, unlike plasma membrane localization of ANX1/2 or RbohH, which shows enrichment at the PT tip (6), MRI-YFP was localized uniformly in the plasma membrane, similar to other pollen-expressed RLCKs (27). Taken together, our results indicate that *mri-1*, *mri-2,* and *mri-3D* are amorphic, hypomorphic, and hypermorphic alleles of *MRI*, respectively, and that disruption of *MRI* leads to a loss of CW integrity during PT growth. Thus, MRI is a positive component of the CW integrity pathway.

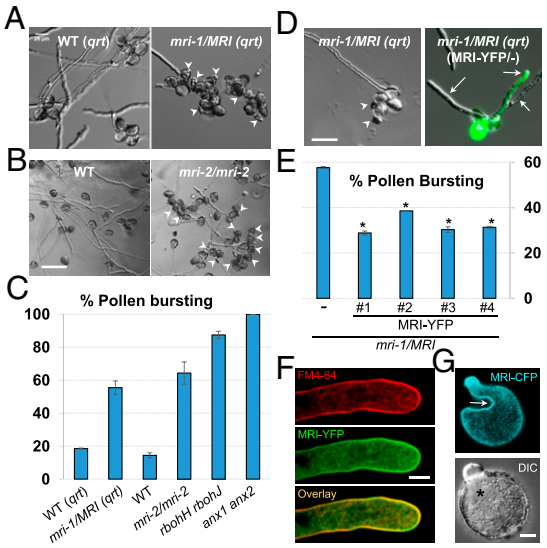

Fig. 2. *MARIS* is a positive component of the CW-integrity signaling pathway. (*A*) In vitro PT growth assays of WT and *mri-1/MRI* in the *qrt* background. Arrowheads point to rupturing PTs discharging cytoplasm into the medium. (Scale bar: 25 μm.) (*B*) In vitro PT growth assays of WT and *mri-2/mri-2*; arrowheads point to cytoplasmic discharge. (Scale bar: 100 μm.) (*C*) Quantification of PT rupture in vitro for WT (*qrt*), *mri-1/MRI* (*qrt*), WT, *mri-2*, *rbohH rbohJ*, and *anx1 anx2*. (*D*) Pollen tetrad of untransformed *mri-1/MRI* (*qrt*) and *mri-1/MRI* (*qrt*) hemizygous for pLAT52-MRI-YFP. Arrowheads and arrows point to cytoplasmic discharge and PT, respectively. DIC and YFP channels were overlaid for the transgenic line. (Scale bar: 50 μm.) (*E*) Four independent T1 lines of *mri-1/MRI* (*qrt*) hemizygous for pLAT52-MRI-YFP display significantly less bursting than untransformed *mri-1/MRI* (*qrt*) (-). Asterisks indicate significant differences from the untransformed control ($P < 0.001$, Student's *t* test). (*F*) Median plane of a normally growing PT expressing MRI-YFP. Before imaging, PTs were treated with liquid germination medium containing FM4-64 (2 μM) for 5 min. (Scale bar: 5 μm.) (*G*) An early arrested PT overexpressing MRI-CFP showing membrane invagination (arrow) and overaccumulation of CW material (asterisk). (Scale bar: 5 μm.)

Overexpression of the MRI^{R240C} Mutant Form Strongly Inhibits WT Pollen Germination. To study the effect of the R240C mutant form further, WT plants were transformed with both MRI-CFP and MRI^{R240C}-CFP. Previously, we reported that overexpression of *ANX1* mildly inhibits pollen germination and PT growth, most likely by triggering overaccumulation of secreted CW material (6). In transgenic lines with strong expression of MRI-CFP, only a few pollen grains displayed membrane invaginations and CW accumulation ($n = 31$ of 444 fluorescent PTs) (Fig. 2*G*). The occurrence of this phenotype was similar in lines strongly expressing GFP-RbohH (6) but was much lower than in the ANX1-OX lines ($n = 65$ of 133). This result suggests that the levels of MRI (and RbohH) do not constitute a rate-limiting step in the pathway. Furthermore, 32 homozygous individuals could be identified among 102 Basta-resistant T2 progenies expressing MRI-CFP (three independent transgenic lines). In contrast, no homozygous individual could be retrieved among 106 Basta-resistant T2 progenies expressing the MRI^{R240C}-CFP fusion (three independent transgenic lines), suggesting that MRI^{R240C}-CFP PTs cannot effect fertilization. To investigate this hypothesis further, we compared in vitro germination and growth of pollen from transgenic lines hemizygous for MRI^{R240C}-CFP and MRI-CFP.

For the latter, MRI-CFP–expressing and nonfluorescent WT PTs were observed in a 1:1.64 ratio, which is significantly different from the expected 1:1 ratio for plants hemizygous for a PT-expressed marker ($P = 0.0022$, two-tailed Fisher's exact test, $n = 330$) (Fig. 3*A*), suggesting that MRI-CFP partially inhibits pollen germination. Remarkably, only two very small fluorescent bulges were observed for plants hemizygous for MRI^{R240C}-CFP ($P < 0.0001$, two-tailed Fisher's exact test, $n = 240$) (Fig. 3*A*). This finding was confirmed further by the decreased or almost absent male TE of the MRI-CFP and MRI^{R240C}-CFP transgenes, respectively (TE_{male} for MRI-CFP = 55.7%, $n = 503$; TE_{male} for MRI^{R240C}-CFP = 5.7%, $n = 258$). Our results show that, in a WT background, overexpression of *MRI* and *MRI^{R240C}* slightly or strongly inhibits pollen germination, respectively, and that they are detrimental to fertilization. These data further indicate that MRI^{R240C} is more active than WT MRI, at least in rescuing *anx1 anx2* sterility and inhibiting PT emergence in a WT background.

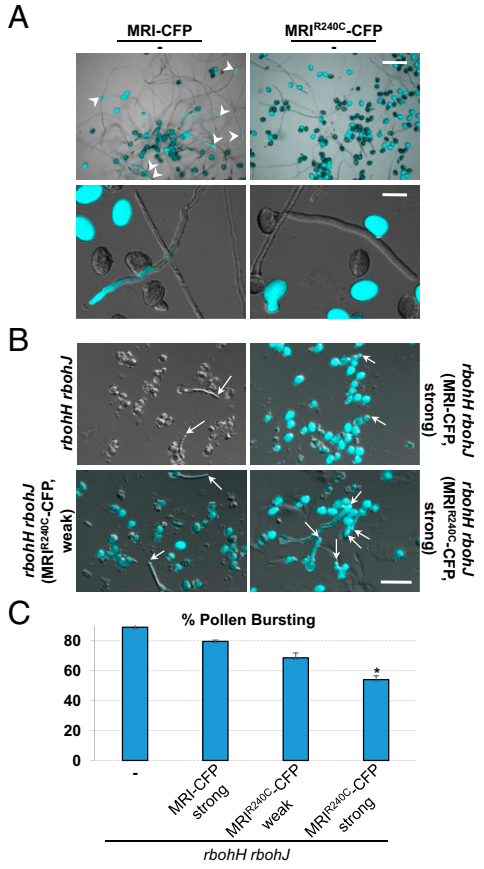

Fig. 3. MRI^{R240C}-CFP strongly inhibits WT pollen germination and partially rescues the *rbohH rbohJ* bursting phenotype. (*A*) In vitro growth assays with WT pollen hemizygous for either MRI-CFP (*Left*) or MRI^{R240C}-CFP (*Right*). DIC and CFP channels were overlaid. (*Upper*) An overview of the growing PTs. Note that, unlike MRI^{R240C}-CFP–expressing PTs (*Right*), MRI-CFP expressing PTs (*Left*) are observed frequently (arrowheads). (*Lower*) Close-up pictures of growing pollen expressing MRI-CFP (*Left*) and very rarely germinating pollen expressing MRI^{R240C}-CFP (*Right*). (Scale bars: 100 μm, *Upper*; 30 μm, *Lower*.) (*B*) In vitro growth assays for untransformed *rbohH rbohJ* pollen (*Upper Left*) and transgenic *rbohH rbohJ* pollen strongly expressing MRI-CFP (*Upper Right*) or weakly (*Lower Left*) or strongly (*Lower Right*) expressing MRI^{R240C}-CFP. DIC and CFP channels were overlaid. Strongly expressed MRI^{R240C}-CFP significantly rescued the *rbohH rbohJ* bursting phenotype in vitro. (Scale bar: 30 μm.) (*C*) Quantification of the bursting phenotype relative to *B*. The asterisk denotes a significant difference compared to untransformed *rbohH rbohJ* PTs (–) ($P < 0.001$, two-tailed unpaired Student's *t* test).

MRI Functions Downstream of ROS-Producing NADPH Oxidases. To position *MRI* in the *ANX1/2* signaling pathway, we tested whether overexpression of *MRI* and *MRI^{R240C}* could rescue partially male-sterile *rbohH rbohJ* mutant plants (6). All 32 independent T1 lines of *rbohH rbohJ* with MRI-CFP fluorescence remained partially sterile (e.g., for three independent T1 lines with high CFP expression, seed set was 8.5 ± 3.1, 8.8 ± 3.9, and 9.4 ± 4.2) similar to untransformed *rbohH rbohJ* plants (7.2 ± 2.1). In contrast, all of the 32 independent T1 lines of *rbohH rbohJ* with MRI^{R240C}-CFP fluorescence produced elongated siliques with many more seeds (e.g., for three independent T1 lines, seed set was 23 ± 3.5, 28.6 ± 4.1, and 30.2 ± 4.9). In the next generation, we recovered a weak and a strong expressor of MRI^{R240C}-CFP, both of which were fertile despite the *rbohH rbohJ* mutations (seed set of 25.6 ± 3.9 and 32.2 ± 3.7, respectively), and we compared their in vitro PT bursting rates with that of a strong MRI-CFP expressor (seed set of 4.6 ± 3.9). PTs from *rbohH rbohJ* plants homozygous for MRI-CFP or untransformed controls burst more frequently in vitro than PTs from *rbohH rbohJ* fertile plants homozygous for MRI^{R240C}–CFP, although only the bursting rate of the strong MRI^{R240C}–CFP line was significantly lower ($P < 0.001$, two-tailed unpaired Student's *t* test) (Fig. 3 *B* and *C*). These results show that hyperactive MRI^{R240C}, but not WT MRI, can partially rescue *rbohH rbohJ* male sterility in vivo and in vitro. Thus, MRI acts downstream of both the ANX-RLKs and the NADPH oxidases to control CW integrity in PTs.

MRI Functions Downstream of FER in Root-Hair Growth Control. Unlike *ANX1/2* and *RbohH/J*, *MRI* displays significant expression in root hairs, another plant cell type with tip growth (Table S1). Because it was reported that *FER* and *RbohC* (analogous to *ANX1/2* and *RbohH/J*) functions to maintain root-hair integrity during growth (19), we tested whether MRI could also play a role in root-hair growth. First, we measured root-hair length in 5-d-old seedlings grown in agar and homozygous for *mri-2* (vs. WT Col-0) and in seedlings homozygous for *mri-1* whose male sterility was complemented with the pollen-preferential expression of pACA9-MRI-YFP (vs. WT L*er*; see *SI Materials and Methods*). Both the *mri-1* and *mri-2* alleles showed much shorter root hairs than their respective WT controls (Fig. 4 *A* and *B*), similar to, but not as short as, the root hairs of plants homozygous for the *fer-1* (L*er*) (11) and *fer-4* (Col-0) (19) alleles. Surprisingly, the strong *mri-1* allele displayed a weaker phenotype in root hairs than the weak *mri-2* allele. However, the *pACA9* promoter also drives weak expression in root hairs (Table S1). It is possible that weak, undetectable expression of MRI-YFP in *mri-1* root hairs may partially complement the short-root-hair phenotype. Moreover, in contrast to *anx1 anx2* and WT seedlings grown on microagar, *mri-3D* seedlings expressing the MRI^{R240C} protein in the *anx1 anx2* background did not have any elongated root hairs (Fig. 4*C*). Microscopic observations of root hairs grown in liquid medium showed that, like *fer-4* root hairs, *mri-2* root hairs were bursting, whereas *mri-3D* short root hairs displayed over-accumulation of pectinaceous CW material (Fig. 4*D*, Figs. S3 and S4, and Movie S1). Taken together, our results show that MRI is essential for PT and root-hair CW integrity, whereas MRI^{R240C} strongly inhibits the growth of both PTs and root hairs. Finally, independent T1 *fer-4* seedlings expressing pMRI-MRI^{R240C}-YFP displayed partial rescue of *fer-4* root-hair phenotype (Fig. 4*E*), indicating that, in root hairs, MRI is a downstream component of FER signaling.

Discussion

During growth, any chemical or physical perturbation of the CW caused by developmental signals, abiotic stresses, and interactions with neighboring cells or microorganisms can potentially cause a cell to stop growing or lose its integrity. For the fast-growing PTs, this growth cessation would lead to a failure in fertilization, necessitating a robust signal transduction network to maintain CW integrity during tip growth.

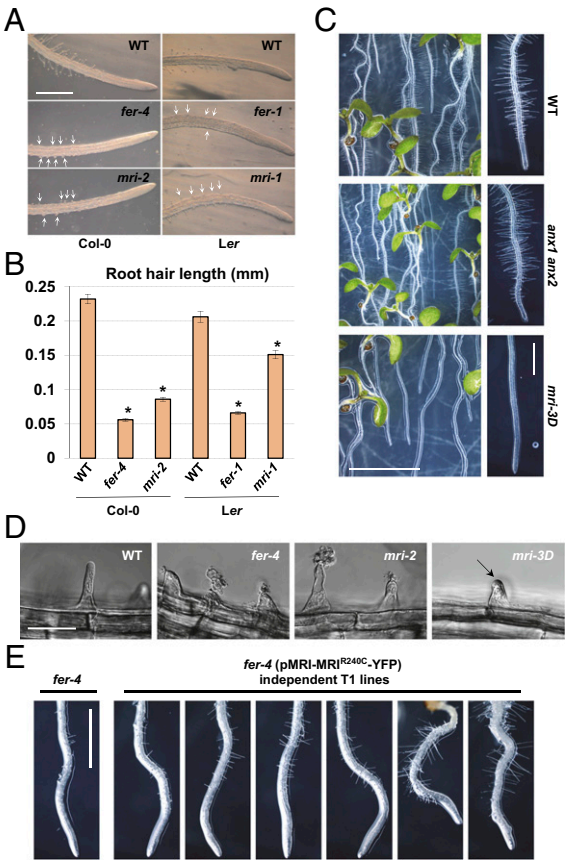

Fig. 4. As in *FERONIA*, *MARIS* is required to sustain root-hair growth. (*A*) Main roots with root hairs of 5-d-old *mri-2*, *fer-4*, and WT (Col-0 accession) seedlings (*Left*) and *mri-1*, *fer-1*, and WT (*Ler* accession) seedlings (*Right*) grown in agar. Arrows point to short, defective root hairs. (Scale bar: 1 mm.) (*B*) Quantification of root-hair lengths relative to *A*. Asterisks denote significant differences versus the appropriate control ($P < 0.001$, two-tailed unpaired Student's *t* test). (*C*, *Left*) WT, *anx1 anx2*, and *mri-3D anx1 anx2* seedlings growing on the surface of a microagar plate. (*Right*) Pictures of primary roots and their root hairs. (Scale bars: 5 mm, *Left*; 1 mm, *Right*.) (*D*) Young root hairs in the root elongation zone of WT, *mri-2*, and *mri-3D anx1 anx2* seedlings grown in liquid medium. Note the loss of CW integrity or CW overaccumulation (arrow) for *mri-2* and *mri-3D* root hairs, respectively. (Scale bar: 20 μm.) See also Figs. S3 and S4 and Movie S1. (*E*) Main root of untransformed *fer-4* seedling and *fer-4* T1s expressing pMRI-MRI^{R240C}-YFP. (Scale bar: 1 mm.)

The ANX1/2 RLKs of the *Cr*RLK1L subfamily and their closest homolog FER have been implicated in the control of tip growth in PTs and root hairs, respectively, acting upstream of ROS-producing NADPH oxidases (3, 4, 19). In this study, we identified MRI, a novel, positive downstream component of these RLK signaling pathways. MRI belongs to the *Arabidopsis* RLCK-VIII subfamily that shares homology with the tomato Pti1 protein involved in the Pto-mediated hypersensitive response (28). In tomato, the Pto kinase interacts with and transphorylates Pti1 in the amino acid motif STR at threonine 233; the biological relevance of this interaction awaits further studies (29). In *Arabidopsis*, four members of the RLCK-VIII subfamily, namely Pti1-1 (AT1G06700), Pti1-2 (AT2G30740), Pti1-3 (AT3G59350), and Pti1-4 (AT2G47060), interact with the AGC2 kinase OXIDATIVE SIGNAL-INDUCIBLE1 (OXI1) (30, 31). However, only Pti1-1, Pti1-2, and Pti1-4 appear to be phosphorylated by OXI1 (30, 31). Interestingly, Pti1-2 and OXI1 kinase activities are induced by ROS-generating stresses (30, 32). The *Arabidopsis oxi1* mutant is more susceptible to pathogens and displays mild root-hair growth defects and less lignin deposition after CW damage (22, 32–34). However, to date no mutant phenotype has been reported for any *Arabidopsis* gene encoding a RLCK-VIII protein.

Here, we show that MRI, a member of the RLCK-VIII subfamily, is preferentially expressed in root hairs and PTs and localizes uniformly at the plasma membrane. Disruption of *MRI* leads to PT bursting similar to that observed in *anx1 anx2* mutants and to root-hair bursting similar to that seen in *fer* homozygous plants. Furthermore, an R240C amino acid substitution in the activation loop of MRI is sufficient for partial rescue of both the *anx1 anx2* and the *rbohH rbohJ* PT-bursting phenotypes and the *fer-4* root-hair–bursting phenotype. Thus, although it is not known whether MRI kinase activity is activated by ROS similar to Pti1-2 (30), our data show that MRI controls CW integrity downstream of ANX1/2 and the NADPH oxidases in PTs and downstream of FER in root hairs. Because OXI1 also is involved in root-hair growth and can phosphorylate different members of the RLCK-VIII subfamily, OXI1 is likely to activate MRI during root-hair growth. In PTs, however, *OXI1* expression levels are very low, and it seems more likely that either another member of this family, the AGC2 kinases (group VIII), or a combination of them fulfills this role (Table S5) (35–37). Whether *Cr*RLK1Ls, NADPH oxidases, OXI1/AGC2 kinases, and MRI/Pti1-like proteins are all part of a linear pathway or, more likely, belong to different pathways that orchestrate complex cross-talk to sustain cell growth remains to be addressed. In this regard, the presence of a module composed of OXI/AGC2 kinases and MRI/Pti1-like RLCKs acting downstream of the *Cr*RLK1Ls and NADPH oxidases could potentially allow the integration of inputs generated by biotic or abiotic stresses with the CW integrity pathway (36, 37).

Interestingly, in all the different genetic backgrounds tested, MRI^{R240C} is more efficient than the WT form in activating downstream responses. The question of how the R240C substitution makes MRI more active is intriguing, and several scenarios can be envisioned. First, this amino acid change in the core catalytic domain may enhance MRI kinase activity itself. Second, MRI^{R240C} could be more resistant than MRI to either degradation or inactivation mechanisms. Third, the interaction of MRI^{R240C} with upstream activators or downstream signaling components could be stronger than that of the WT form, resulting in more efficient activation of the downstream responses. In this respect it is noteworthy that, in tomato, Pto phosphorylates Pti1 at T233 in the conserved STR motif of RLCKs-VIII (29), but in *Arabidopsis*, OXI1 phosphorylates Pti1-2 at T238 (30). In MRI, the corresponding conserved threonine is located at position 239, just before R240, which is mutated in *mri-3D* (Fig. 1*C* and Fig. S1*B*). Therefore it is conceivable that the R240C substitution in MRI facilitates phosphorylation at the neighboring T239 or partially mimics a phosphorylated T239, enabling MRI^{R240C} to be more efficient than MRI in activating downstream components. Future studies combining biochemistry and rescue experiments of mutants in these signaling pathways will be needed to distinguish which of these scenarios best explains the phenotypes triggered by *MRI^{R240C}* expression. We anticipate that engineering and expressing this type of mutation in the conserved STR motif could be very useful for studying the other unexplored RLCK-VIII–mediated signaling pathways.

Materials and Methods

Plant Material, Growth Conditions, and Genotyping of Mutant Alleles. Mutant lines *mri-1* and *mri-2* with insertions in the *MRI* gene (*At2g41970*) were obtained from Cold Spring Harbor Laboratory and the European *Arabidopsis* Stock Center and correspond to CSHL_GT21229 (*Ds* element inserted 1,632 bp downstream of the start codon, *Ler* accession, kanamycin resistance) and GABI_820D05 (T-DNA insertion located 360 bp upstream of the start codon, Col-0 accession, sulfadiazine resistance), respectively (Table S6 and *SI Materials and Methods*).

In Vitro Pollen Growth Assays. In vitro pollen growth assays were carried out as described previously (38). Briefly, freshly opened flowers were incubated at 22 °C for 30 min in moisture incubation boxes and then were brushed on slides containing germination medium [0.01% boric acid, 5 mM $CaCl_2$, 5 mM KCl, 1 mM $MgSO_4$, 10% (wt/vol) sucrose (pH 7.5), 1.5% (wt/vol) low-melting agarose]. The boxes were preincubated for 35 min at 30 °C and then were returned to 22 °C for several hours. To determine the percentage of bursting PTs, germinating pollen grains and PTs were imaged with a Leica DM6000 microscope and were analyzed using the ImageJ 1.47d software (rsb.info.nih.gov/ij). All data presented here are the mean ± SEM of three independent experiments with more than 150 pollen grains (or 30 tetrads for the *qrt* background) scored per genotype and experiment.

Analysis of Root-Hair Length. Root hairs located 1.5–3.5 mm from the primary root tip of 5-d-old seedlings grown in half-strength MS medium (1% sucrose) were observed with a Leica MZ16F stereomicroscope. The length of ∼100 root hairs in focus from at least 18 seedlings per genotype was measured with ImageJ 1.47d. Data are presented as the mean ± SEM of three independent experiments with more than 30 root hairs scored per genotype and experiment. Alternatively, roots from 7-d-old seedlings grown on microagar plates were imaged. For microscopic root-hair observations, 4-d-old seedlings grown on half-strength MS microagar plates were sandwiched between a slide and a coverslip containing 1/10th strength MS liquid medium supplemented with 1% sucrose (Fig. S3). Emerging root hairs were observed 48 h later with a Leica DM5500 equipped with differential interference contrast (DIC) optics.

ACKNOWLEDGMENTS. We thank all members of the U.G. and Martin Hülskamp laboratories for help with mutant screening and enriching discussions, in particular Rita Galhano, Sharme Thirugnanarajah, Sucharita Roy, and the Plant Sex Club; the Functional Genomics Center Zurich and its staff for deep-sequencing of the *mri-3D/MRI* mutant; Sharon Kessler (University of Oklahoma), Michael R. Sussman, and Miyoshi Haruta (University of Wisconsin) for *fer* seeds; Yan Zhang (Shandong Agricultural University) for plasmids; and Boris Voigt (University of Bonn) for fruitful suggestions about live imaging of root hairs. This work was supported by the University of Zurich; by grants from the University of Zurich's Research Priority Program "Functional Genomics/Systems Biology," the European Union through the Marie Curie International Reintegration Grant FP7-PEOPLE-2009-RG (project 249247) and the PLANTFELLOWS Grant GA-2010-267243, and the Deutsche Forschungsgemeinschaft Grant BO 4470/1-1 (to A.B.-D.); as well as by Swiss National Science Foundation Grant 31003A-112489; an interdisciplinary PhD project from SystemsX.ch; and European Research Council Grant AdG 250358 (to U.G.).

1. Engelsdorf T, Hamann T (2014) An update on receptor-like kinase involvement in the maintenance of plant cell wall integrity. *Ann Bot (Lond)* 114(6):1339–1347.
2. Wolf S, Hématy K, Höfte H (2012) Growth control and cell wall signaling in plants. *Annu Rev Plant Biol* 63:381–407.
3. Boisson-Dernier A, et al. (2009) Disruption of the pollen-expressed *FERONIA* homologs *ANXUR1* and *ANXUR2* triggers pollen tube discharge. *Development* 136(19): 3279–3288.
4. Miyazaki S, et al. (2009) *ANXUR1* and *2*, sister genes to *FERONIA/SIRENE*, are male factors for coordinated fertilization. *Curr Biol* 19(15):1327–1331.
5. Lindner H, et al. (2015) TURAN and EVAN mediate pollen tube reception in *Arabidopsis* synergids through protein glycosylation. *PLoS Biol* 13(4):e1002139.
6. Boisson-Dernier A, et al. (2013) ANXUR receptor-like kinases coordinate cell wall integrity with growth at the pollen tube tip via NADPH oxidases. *PLoS Biol* 11(11): e1001719.
7. Boisson-Dernier A, Kessler SA, Grossniklaus U (2011) The walls have ears: The role of plant *Cr*RLK1Ls in sensing and transducing extracellular signals. *J Exp Bot* 62(5): 1581–1591.
8. Lindner H, Müller LM, Boisson-Dernier A, Grossniklaus U (2012) *Cr*RLK1L receptor-like kinases: Not just another brick in the wall. *Curr Opin Plant Biol* 15(6):659–669.
9. Cheung AY, Wu H-M (2011) THESEUS 1, FERONIA and relatives: A family of cell wall-sensing receptor kinases? *Curr Opin Plant Biol* 14(6):632–641.
10. Ngo QA, Vogler H, Lituiev DS, Nestorova A, Grossniklaus U (2014) A calcium dialog mediated by the *FERONIA* signal transduction pathway controls plant sperm delivery. *Dev Cell* 29(4):491–500.
11. Escobar-Restrepo J-M, et al. (2007) The FERONIA receptor-like kinase mediates male-female interactions during pollen tube reception. *Science* 317(5838):656–660.
12. Duan Q, et al. (2014) Reactive oxygen species mediate pollen tube rupture to release sperm for fertilization in *Arabidopsis*. *Nat Commun* 5:3129.
13. Guo H, et al. (2009) Three related receptor-like kinases are required for optimal cell elongation in *Arabidopsis thaliana*. *Proc Natl Acad Sci USA* 106(18):7648–7653.
14. Deslauriers SD, Larsen PB (2010) FERONIA is a key modulator of brassinosteroid and ethylene responsiveness in *Arabidopsis* hypocotyls. *Mol Plant* 3(3):626–640.
15. Yu F, et al. (2012) FERONIA receptor kinase pathway suppresses abscisic acid signaling in *Arabidopsis* by activating ABI2 phosphatase. *Proc Natl Acad Sci USA* 109(36): 14693–14698.
16. Shih H-W, Miller ND, Dai C, Spalding EP, Monshausen GB (2014) The receptor-like kinase FERONIA is required for mechanical signal transduction in *Arabidopsis* seedlings. *Curr Biol* 24(16):1887–1892.
17. Kessler SA, et al. (2010) Conserved molecular components for pollen tube reception and fungal invasion. *Science* 330(6006):968–971.
18. Keinath NF, et al. (2010) PAMP (pathogen-associated molecular pattern)-induced changes in plasma membrane compartmentalization reveal novel components of plant immunity. *J Biol Chem* 285(50):39140–39149.
19. Duan Q, Kita D, Li C, Cheung AY, Wu H-M (2010) FERONIA receptor-like kinase regulates RHO GTPase signaling of root hair development. *Proc Natl Acad Sci USA* 107(41):17821–17826.
20. Haruta M, Sabat G, Stecker K, Minkoff BB, Sussman MR (2014) A peptide hormone and its receptor protein kinase regulate plant cell expansion. *Science* 343(6169): 408–411.
21. Kessler SA, Lindner H, Jones DS, Grossniklaus U (2015) Functional analysis of related *Cr*RLK1L receptor-like kinases in pollen tube reception. *EMBO Rep* 16(1):107–115.
22. Denness L, et al. (2011) Cell wall damage-induced lignin biosynthesis is regulated by a reactive oxygen species- and jasmonic acid-dependent process in *Arabidopsis*. *Plant Physiol* 156(3):1364–1374.
23. Gerhard E (1847) *Über die Gottheiten der Etrusker* (Druckerei der Königlichen Akademie der Wissenschaften, Berlin).
24. Lindner H, et al. (2012) SNP-Ratio Mapping (SRM): Identifying lethal alleles and mutations in complex genetic backgrounds by next-generation sequencing. *Genetics* 191(4):1381–1386.
25. Twell D, Yamaguchi J, Wing RA, Ushiba J, McCormick S (1991) Promoter analysis of genes that are coordinately expressed during pollen development reveals pollen-specific enhancer sequences and shared regulatory elements. *Genes Dev* 5(3): 496–507.
26. Preuss D, Rhee SY, Davis RW (1994) Tetrad analysis possible in *Arabidopsis* with mutation of the *QUARTET* (*QRT*) genes. *Science* 264(5164):1458–1460.
27. Liu J, et al. (2013) Membrane-bound RLCKs LIP1 and LIP2 are essential male factors controlling male-female attraction in *Arabidopsis*. *Curr Biol* 23(11):993–998.
28. Zhou J, Loh Y-T, Bressan RA, Martin GB (1995) The tomato gene *Pti1* encodes a serine/threonine kinase that is phosphorylated by Pto and is involved in the hypersensitive response. *Cell* 83(6):925–935.
29. Sessa G, D'ascenzo M, Martin GB (2000) The major site of the Pti1 kinase phosphorylated by the Pto kinase is located in the activation domain and is required for Pto-Pti1 physical interaction. *Eur J Biochem* 267(1):171–178.
30. Anthony RG, Khan S, Costa J, Pais MS, Bögre L (2006) The *Arabidopsis* protein kinase PTI1-2 is activated by convergent phosphatidic acid and oxidative stress signaling pathways downstream of PDK1 and OXI1. *J Biol Chem* 281(49):37536–37546.
31. Forzani C, et al. (2011) The *Arabidopsis* protein kinase Pto-interacting 1-4 is a common target of the oxidative signal-inducible 1 and mitogen-activated protein kinases. *FEBS J* 278(7):1126–1136.
32. Rentel MC, et al. (2004) OXI1 kinase is necessary for oxidative burst-mediated signalling in *Arabidopsis*. *Nature* 427(6977):858–861.
33. Anthony RG, et al. (2004) A protein kinase target of a PDK1 signalling pathway is involved in root hair growth in *Arabidopsis*. *EMBO J* 23(3):572–581.
34. Petersen LN, Ingle RA, Knight MR, Denby KJ (2009) OXI1 protein kinase is required for plant immunity against *Pseudomonas syringae* in *Arabidopsis*. *J Exp Bot* 60(13): 3727–3735.
35. Enugutti B, et al. (2012) Regulation of planar growth by the *Arabidopsis* AGC protein kinase UNICORN. *Proc Natl Acad Sci USA* 109(37):15060–15065.
36. Rademacher EH, Offringa R (2012) Evolutionary adaptations of plant AGC kinases: From light signaling to cell polarity regulation. *Front Plant Sci* 3:250.
37. Garcia AV, Al-Yousif M, Hirt H (2012) Role of AGC kinases in plant growth and stress responses. *Cell Mol Life Sci* 69(19):3259–3267.
38. Boavida LC, McCormick S (2007) Temperature as a determinant factor for increased and reproducible *in vitro* pollen germination in *Arabidopsis thaliana*. *Plant J* 52(3): 570–582.
39. Sedlazeck FJ, Rescheneder P, von Haeseler A (2013) NextGenMap: Fast and accurate read mapping in highly polymorphic genomes. *Bioinformatics* 29(21):2790–2791.
40. Li H, et al.; 1000 Genome Project Data Processing Subgroup (2009) The Sequence Alignment/Map format and SAMtools. *Bioinformatics* 25(16):2078–2079.
41. Barnett DW, Garrison EK, Quinlan AR, Strömberg MP, Marth GT (2011) BamTools: A C++ API and toolkit for analyzing and managing BAM files. *Bioinformatics* 27(12): 1691–1692.
42. Erik G, Gabor M (2012) Haplotype-based variant detection from short-read sequencing. Available at arxiv.org/pdf/1207.3907.pdf. Accessed May 14, 2015.
43. Myers C, et al. (2009) Calcium-dependent protein kinases regulate polarized tip growth in pollen tubes. *Plant J* 59(4):528–539.
44. Karimi M, De Meyer B, Hilson P (2005) Modular cloning in plant cells. *Trends Plant Sci* 10(3):103–105.
45. Hruz T, et al. (2008) Genevestigator v3: A reference expression database for the meta-analysis of transcriptomes. *Adv Bioinforma* 2008:420747.
46. Loraine AE, McCormick S, Estrada A, Patel K, Qin P (2013) RNA-seq of *Arabidopsis* pollen uncovers novel transcription and alternative splicing. *Plant Physiol* 162(2): 1092–1109.
47. Honys D, Twell D (2004) Transcriptome analysis of haploid male gametophyte development in *Arabidopsis*. *Genome Biol* 5(11):R85.
48. Becker JD, Takeda S, Borges F, Dolan L, Feijó JA (2014) Transcriptional profiling of *Arabidopsis* root hairs and pollen defines an apical cell growth signature. *BMC Plant Biol* 14:197.